

An International Ultraviolet Explorer Archival Study of Dwarf Novae in Outburst

Ryan T. Hamilton, Joel A. Urban, Edward M. Sion, Adric R. Riedel, Elysse N. Voyer, John T. Marcy, Sarah L. Lakatos

Dept of Astronomy & Astrophysics, Villanova University, Villanova, PA 19085, e-mail:
ryan.hamilton@villanova.edu, jurban@ast.vill.edu, emsion@ast.vill.edu,
adric.riedel@villanova.edu, elysse.voyer@villanova.edu, john.marcy@villanova.edu
sarah.lakatos@villanova.edu

ABSTRACT

We present a synthetic spectral analysis of nearly the entire far ultraviolet International Ultraviolet Explorer (IUE) archive of spectra of dwarf novae in or near outburst. The study includes 46 systems of all dwarf nova subtypes both above and below the period gap. The spectra were uniformly analyzed using synthetic spectral codes for optically thick accretion disks and stellar photospheres along with the best-available distance measurements or estimates. We present newly estimated accretion rates and discuss the implications of our study for disk accretion physics and CV evolution.

Subject headings: Stars: white dwarfs, stars: dwarf novae, accretion disks

1. Introduction

Dwarf novae (DNe) are a subclass of cataclysmic variables (CVs), comprised of a low-mass, main sequence secondary star and a white dwarf (WD) primary. They are characterized by their quasi-periodic outburst episodes that are typically 2-6 mag in amplitude. The Roche lobe-filling secondary loses gas through the inner langrangian point carrying substantial angular momentum that leads to the formation of a disk around the accreting white dwarf. A thermal-viscous instability known as the disk instability model (Osaki 2005 and references therein) causes the accretion disk to transition from a cool, quiescent, optically thin state to a stable state where the disk is much hotter, more luminous, optically thick and approaching a steady state. The disk is heated due to the release of gravitational potential energy as the accreted material spirals through the optically thick disk toward the WD surface. The energy released can heat the disk to temperatures on the order of 100,000 K. This heating

of the disk accounts for the increase in luminosity during a dwarf nova (DN) outburst, and should dominate the system’s luminosity in outburst. When the outburst concludes, the disk should, theoretically, be relatively empty of material in its hotter inner regions and optically thin. At this time, the disk luminosity should be a negligible contributor to the system’s luminosity. This period of low mass-transfer is known as quiescence.

In dwarf novae, it has long been noted that the systems generally undergo a transition from emission line-dominated spectra in the optical and UV (in quiescence) to absorption line spectra as the continuum gradually increases in strength up to outburst maximum with the development of broad absorption troughs and in the UV, P Cygni profile structure in the resonance lines. In the optical, emission line cores remain but have narrower widths than their counterparts in quiescence (Warner 1995 and references therein). The spectra in outburst and quiescence exhibit a mix of H and He lines as well as metals, unlike the dichotomy between the DA (H-rich) and DB (He-rich) composition sequences of the isolated white dwarfs.

Two types of dwarf nova outbursts have been recognized, Type A, which have a fast optical rise, delay progressively at shorter wavelengths and describe a wide loop in the two color diagram as the system progresses from quiescence to outburst, then back to quiescence, and Type B, in which the optical rise is slower and the cycle describes a narrow loop in the two color diagram with only a small or zero delay between the UV and optical (Smak 1984a,b). On the decline from outburst, systems of both types show fluxes that fall simultaneously at all wavelengths but with the UV declining fastest near the end of the decline. Pringle & Verbunt (1984) and Verbunt (1987) found that the UV flux distributions evolve similarly for a given kind of outburst.

Early attempts to theoretically interpret the spectral energy distributions of dwarf novae in outburst relied on comparisons of the the ratios of continuum fluxes in emission-line free regions with model predictions. The UV flux distributions of DNe in outburst have been mostly fitted with $F_\lambda \simeq \lambda^\alpha$ flux distributions where $\alpha \sim -2$ (Verbunt 1987). Moderately good agreement was achieved for systems expected to approximate steady state disks. The largest uncertainty in the disk model fitting is the sensitivity to the WD mass (Verbunt 1987). The outburst spectra have overall flux distributions that resemble in both the optical and UV, the flux distribution of a B2-3 V-III star ($T_{eff} \sim 20,000\text{K}$).

la Dous (1991) noted in her archival study of 32 dwarf novae in outburst that the UV continuum flux distributions were virtually identical regardless of inclination angle, except for the systems OY Car, Z Cha, AB Dra, WW Cet, CM Del, RX And, and VW Vul (with increasingly bluer distributions but all redder than the bulk of objects) and UZ Ser that is much bluer than the other objects. la Dous (1991) used the published flux plots from an

earlier generation of accretion disk models to conclude that the inner disk radius, inclination angle and mass transfer rate at a fixed WD mass of $1 M_{\odot}$ are the most critical factors in modeling the observed energy distribution. In particular, the appearance of the UV spectra at outburst is strongly correlated with the orbital inclination. In lower inclination systems the outburst spectra appear in pure absorption while for higher inclinations ($70 < i < 80$ degrees) the spectra are continuous and finally for $i > 80$ degrees, strong emission lines are present (la Dous 1991).

Accretion rates have been obtained from absolute magnitudes M_V (requiring distances) for various subgroups of CVs with due account for the sensitivity to system parameters such as the inclination angle (Smak, 1989, 1994). Generally, during dwarf nova maximum, outburst accretion rates have been estimated in the range $\dot{M} = 3 \times 10^{-9}$ to $1 \times 10^{-8} M_{\odot} \text{yr}^{-1}$ while during the rise to outburst among dwarf novae, accretion rates in the range $\dot{M} = 5 \times 10^{-10}$ to $3 \times 10^{-9} M_{\odot} \text{yr}^{-1}$ have been derived (Warner 1995). However, relatively few individual accretion rates have been published for dwarf novae in outburst based upon detailed accretion disk model fitting. There is a comprehensive atlas of optical spectra of dwarf novae in outburst (Morales-Rueda and Marsh 2002) but none for UV spectra in which the data has been modeled and parameters derived. Some examples of early derivations of accretion rates in outburst from disk model fitting are for VW Hyi, Z Cha, OY Car and SS Cygni. For VW Hyi, an accretion rate $\dot{M} = 5 \times 10^{-9} M_{\odot} \text{yr}^{-1}$ was obtained by Polidan, Mauche and Wade (1990), and Polidan and Holberg (1984). For Z Cha, Horne and Cook (1995) obtained $\dot{M} = 2.5 \times 10^{-9} M_{\odot} \text{yr}^{-1}$ and for OY Car, Rutten et al. (1992) obtained $\dot{M} = 1.6 \times 10^{-9} M_{\odot} \text{yr}^{-1}$. For SS Cygni at maximum, Kiplinger (1979) found excellent agreement between a model accretion disk with $\dot{M} = 8.5 \times 10^{-8} M_{\odot} \text{yr}^{-1}$ and the observed flux distribution from the IR through the FUV regions. If \dot{M} is not constant throughout the disk, then steady state disk model fitting in outburst will yield discrepancies due to a non-steady state radial temperature distribution, $T(r)$, in the disk.

Of course, there is a strong sensitivity to the white dwarf mass which is poorly known for the majority of systems. Orbital inclinations are likewise uncertain and distances remain for the most part rough estimates except for less than two dozen systems that have reliable trigonometric parallaxes. Thus, even for a given inclination angle and distance, the accretion disk fits to be described in section 3 yield inferred white dwarf masses uncertain by at least three-tenths of a solar mass. While our spectral coverage is restricted and excludes the regions where the boundary layer and the white dwarf probably contribute to the FUV flux, the International Ultraviolet Explorer (IUE) spectra do cover the range of wavelengths where accretion disks during outburst are emitting a large fraction of their light. In view of all these caveats, our disk model fits should be regarded only as first approximations to the real accretion rates during outburst. Moreover, these spectra nicely complement the compilation

of optical spectra of dwarf novae in outburst described by Morales-Rueda and Marsh (2002).

2. Archival IUE Spectral Data

All the spectral data were obtained from the Multimission Archive at Space Telescope (MAST) IUE archive are in a high activity state, very near or at outburst. We restricted our selection to those systems with SWP spectra, with resolution of 5\AA and a spectral range of 1170\AA to 2000\AA . All spectra were taken through the large aperture at low dispersion. The Massa & Fitzpatrick (2000) flux calibration-correction algorithm was applied to all the IUE data used; please see their paper for a description of the corrections it makes to the data. When more than one spectrum with adequate signal-to-noise ratio was available, the two best spectra were analyzed. An observing log of the observations is given in Table 1, where we list: (1) the system name, (2) data ID, (3) date of observation, (4) Universal Time of observation, (5) exposure time, and (6) activity state. Transition refers to an intermediate state between outburst and quiescence, and an asterisk in the last column indicates that an outburst state was determined without a ground-based optical light curve at the time of the IUE observation.

The activity state of the spectra was determined by examining the AAVSO light curves for each system as well as the flux level of the IUE spectrum that typically made it obvious the spectrum was obtained in outburst. Unfortunately, we were unable to cross-reference this AAVSO data with data from VSNET during the preparation of this paper due to their archives being off-line. In the case of those systems not covered by the AAVSO, their activity state was assessed based upon either mean photometric magnitudes taken from the Ritter & Kolb(2003) catalogue or from IUE Fine Error Sensor (FES) measurements at the time of the IUE observation. The FES counts, when available, were converted to optical magnitudes to help ascertain the brightness state at the time of the IUE observation, and used as consistency checks on our model fitting since the model-predicted optical magnitude from a best-fitting model should always be fainter than observed optical magnitude of the system. This is because of the contribution in the optical of the secondary. In addition, the presence of P-Cygni profiles, absorption lines, and comparison with spectral data and flux levels for the systems during other activity states was used to ascertain the state of the system.

The reddening of the systems was determined based upon all estimates listed in the literature. The three principal sources of reddening were the compilations of la Dous (1991), Verbunt (1987) and Bruch & Engel (1999). If there was a range of values found, then the value we assume in our analyses follows the range shown in Column (7) of Table 2, and the

ranges and assumed values are separated by a semicolon. If only one value was listed in the literature, then we adopted that value, and if there was none listed, we took the reddening to be zero. The spectra were then de-reddened with the IUERDAF routine UNRED.

3. Synthetic Spectral Fitting Procedure

3.1. Distance Constraints on the Fitting

As a constraint on the goodness of a particular model fit, we adopted a distance from either a trigonometric parallax, the Warner (1995) and Harrison et al. (2004) relations or from the scale factor of the best-fitting WD model to HST spectra of dwarf novae during quiescence. The adopted distance was used as a basis for comparison with distances yielded by the accretion disk model fitting. The most direct means of knowing the distance is to have trigonometric parallaxes such as those measured by Thorstensen (2003) for 14 dwarf novae. But dwarf novae and nova-like variables also offer the advantage of estimating distances from correlations between their absolute magnitudes at maximum brightness and their orbital periods. Distance estimates were obtained from either the absolute magnitude at outburst $M_{V(\max)}$ versus orbital period P_{orb} relation of Warner (1995) or from a more recent relationship by Harrison et al. (2004) based upon their recent HST FGS parallaxes of dwarf novae. The Warner (1995) relation is

$$M_{V(\max)} = 5.74 - 0.259P_{orb}(\text{hr}) \quad (1)$$

and the Harrison et al.(2004) relation is

$$M_{V(\max)} = 5.92 - 0.383P_{orb}(\text{hr}) \quad (2)$$

At the outset of the modeling process, we applied both of these relationships to each system. Then, we conducted an exhaustive search of the literature for previous distance estimates. If the literature search revealed other estimates, then we adopted some reasonable mean based upon the different methods used to obtain each distance estimate and the distance computed from the two calibrated $M_{V(\max)} - P_{orb}$ relations. If no other distance estimates existed, then we simply adopted a reasonable mean of the two $M_{V(\max)} - P_{orb}$ relations. If a trigonometric parallax was available, then we adopted it for the distance. In the case of two systems (U Gem and YZ Cnc), there was more than one parallax. For U Gem, all were identical. For YZ Cnc, they were slightly different, so we took a mean of the parallax values. In the case of SU UMa, the parallax obtained was unreliable, so we combined it in a mean with other distances estimates and the $M_{V(\max)} - P_{orb}$ relations. The adopted distances used as constraints in the synthetic spectral fitting procedure are shown in Table 2.

3.2. Synthetic Spectral Fitting

We adopted model accretion disks from the optically thick disk model grid of Wade & Hubeny (1998). In these accretion disk models, the innermost disk radius, R_{in} , is fixed at a fractional white dwarf radius of $x = R_{in}/R_{wd} = 1.05$. The outermost disk radius, R_{out} , was chosen so that $T_{eff}(R_{out})$ is near 10,000K since disk annuli beyond this point, which are cooler zones with larger radii, would provide only a very small contribution to the mid and far UV disk flux, particularly the SWP FUV bandpass. The mass transfer rate is assumed to be the same for all radii. Thus, the run of disk temperature with radius is taken to be:

$$T_{eff}(r) = T_s x^{-3/4} (1 - x^{-1/2})^{1/4} \quad (3)$$

where $x = r/R_{wd}$ and $\sigma T_s^4 = 3GM_{wd}\dot{M}/8\pi R_{wd}^3$

Limb darkening of the disk is fully taken into account in the manner described by Diaz et al. (1996) involving the Eddington-Barbier relation, the increase of kinetic temperature with depth in the disk, and the wavelength and temperature dependence of the Planck function. The boundary layer contribution to the model flux is not included. However, the boundary layer is expected to contribute primarily in the extreme ultraviolet below the Lyman limit.

After masking emission lines, artifacts and poor quality data in the spectra, we determined separately for each system, the best-fitting accretion disk model using IUEFIT, a χ^2 minimization routine. In virtually every dwarf nova system in our IUE sample, the accretion disk by itself provided very good agreement with the outburst spectra. However, if the accretion disk fit to the outburst spectrum was not entirely satisfactory over the entire wavelength range despite the disk providing nearly 100% of the flux, then an attempt was made to slightly improve the fit by adding the flux contribution of a hot white dwarf. For this minority of cases, WD Model spectra with solar abundances were created for high gravity stellar atmospheres using TLUSTY (Hubeny 1988) and SYNSPEC (Hubeny & Lanz 1995). We took a range of gravities in the fitting from $\text{Log } g = 7.0 - 9.0$ in steps of 0.5. For the white dwarf radii, we use the mass-radius relation from the evolutionary model grid of Matt Wood (private communication). These models have realistic non-degenerate H-rich envelopes, use the Lamb and Van Horn equation of state and include the effect of non-zero temperature on the WD radius.

We took the best-fitting accretion disk model and combined it with a hot WD model, using a χ^2 minimization routine called DISKFIT. The best-fitting composite accretion disk plus white dwarf was determined based upon the minimum χ^2 value achieved and consistency of the scale factor-derived distance with the adopted distance for each system. The scale

factor, S , normalized to a kiloparsec and solar radius, can be related to the white dwarf radius R through: $F_{\lambda(obs)} = SH_{\lambda(model)}$, where $S = 4\pi R^2 d^{-2}$, and d is the distance to the source.

An illustration of the accuracy we can obtain in a formal error analysis with confidence contours are given in Winter & Sion (2003). In that paper we presented accretion rates of EM Cygni, CZ Ori and WW Ceti in quiescence, in which 1σ , 2σ and 3σ confidence contours are given. In Table 2, we list the final composite fitting results for all systems, by column, as follows: (1) A reference number, (2) system name, (3) system type (and sub-type, if applicable), (4) P_{orb} , (5) $E(B-V)$, (6) adopted distance, (7) inclination, (8) mass accretion rate \dot{M} , (9) percent flux contribution of the WD, and (10) percent flux contribution of the disk.

The best fitting accretion disk model for each system is shown in the accompanying Figures 1-8, listed in order of increasing orbital period as in Table 2. The thick solid line is the best fitting accretion disk. The accretion disk is the overwhelmingly dominant contributor in the FUV. If in rare cases a hot white dwarf flux contribution was added in an attempt to slightly improve the fits, then the thick solid line represents their combination, the dashed curve represents the accretion disk alone, and the dotted curve represents the white dwarf. Also included are a reference number and name given in Table 2 to clearly identify each system. To discuss a particular system, the figures are labelled Figure N.nn, where N is the figure number and nn is the reference number of a particular dwarf nova.

There are several distances listed in column (6) of Table 2 that are followed by either a π , or a π in parentheses. If the distance is followed by a π , that distance is taken from a parallax (or parallaxes in the case of U Gem). If the distance is followed by a π in parentheses, then it is an adopted distance that incorporates a parallax (see the explanation in section 3.1). All parallaxes are taken from either Harrison et al. (2004), or Thorstensen (2003). A colon in Column 7 denotes an uncertain result.

Although the eclipsing dwarf novae OY Car and Z Cha are part of the IUE archival sample, these systems are not included in the statistics of this study and their derived accretion rates cannot be taken seriously. This is because the accretion disk in these systems is self-eclipsed (i.e. the outer disk obscures the inner disk). Hence, any derived parameters (for example, the accretion rate, percentage of disk flux contribution) are systematically affected.

In Table 2 it is seen that virtually all of the accretion rates derived from the FUV flux distribution with steady state, optically thick disk models fall within the range 1×10^{-8} to $1 \times 10^{-9} M_{\odot} \text{yr}^{-1}$ for the distances, white dwarf masses, orbital inclinations, and interstellar

reddening values we have adopted. This is no great surprise although the range of accretion rates that we derive is somewhat broader than the range derived by Warner (1995) whose accretion rates were based upon the absolute magnitudes of the accretion disk corrected for inclination and limb darkening effects. It should be acknowledged however that some of the distances for the 44 dwarf novae in our study involved the use of the Warner (1995) relation. Hence, the rough agreement with the range of accretion rates found by Warner (1995) from his optical study is biased to some degree in favor of such an agreement. Moreover, as is well known, in all of the outburst spectra, almost without exception, N V (1238Å, 1242Å), C IV (1548Å, 1550Å) and Si IV (1393Å, 1402Å), the hallmark resonance doublets are seen in prominent blue-shifted absorption and originate in the CV wind. In many of the hotter disk models, one sees synthetic Si IV absorption but the disk temperatures are not high enough for significant non-wind C IV, N V or O V. The strongest metallic absorption seen in the spectra, aside from the wind resonance doublets, is due to a blend of multiplet 2 of Si III (1300Å), Si II and O I (1302Å). In virtually all of the model accretion disk fits, the observed absorption centered at 1300Å is reasonably well represented by the synthetic disk Si III absorption at the solar abundance of silicon. A difficulty of fitting the width of the Lyman α profiles in most of the outburst spectra is the presence of N V which complicates discerning the longward wing of Lyman α . Fortunately, the shortward wing is usually quite apparent and one can assume, as a first approximation, mirror symmetry between the two wings. Nonetheless, in some cases the N V looks suspiciously like a pseudo-absorption feature created by the geocoronal emission reversal seen in the core of Lyman α .

Several individual spectra are noteworthy for reasons other than just the goodness of their fit with steady state, optically thick accretion disk energy distributions. In Figure 1.02, the outburst spectrum of the SU UMa system SW UMa along with the best-fitting accretion disk model. There are profiles (e.g. C IV 1550Å, Si II 1260Å) which appear to have emission flanking absorption on both the shortward and longward sides of the absorption. Similar profile shapes were seen during the early stages of the July 2001 superoutburst of WZ Sge (Sion et al.2003). The emission seen near C IV could well be due to the Si II (1526Å, 1533Å) doublet, which would match the same structure seen at Si II (1260Å). If this is the case, then C IV is barely seen and may be very weak relative to nitrogen.

In Figures 1.04, 3.16, 4.18, 6.33, 7.35, 7.39, 7.40, 8.41, 8.42, 8.43, and 8.44, the outburst spectra of T Leo, WX Hyi, YZ Cnc, RX And, AH Her, Z Cam, EM Cyg, RU Peg, SY Cnc, DX And, and BV Cen, respectively, reveal a deviation from a steady state flux distribution longward of 1700Å. In every case, the disk model flux is lower than the observed flux. The deviation tends to be more pronounced among Z Cam-type systems. A anonymous referee suggests this may be due to the secondary star or possibly a shortfall of flux due to the temperature of the outermost disk boundary being set at 10,000K. In our sample, except for

T Leo, this deviation is seen primarily in systems above the period gap.

As stated earlier, one difficulty of fitting the width of the Lyman α profiles in this and other outburst spectra is the presence of N V (1238Å, 1242Å) which in some cases may actually be a pseudo-feature created by the geocoronal emission reversal seen in the core of Lyman α . In Figure 2.09, TV Crv has an unusually strong Si IV (1393Å, 1402Å) absorption suggesting possible suprasolar Si abundance or a higher Si IV ionization fraction in the outflowing wind material.

4. Discussion

Our analyses represent the first detailed look at all of the dwarf novae observed with the IUE SWP in outburst in a systematic way. We have applied a uniform analysis to the largest spectroscopic sample of FUV spectra of dwarf novae, obtained during the same brightness state with the same telescope, and the same instrumental setup, taking into the account the best available distance information. Accordingly, this large body of accretion rates will serve as a basis of comparison with accretion rates derived by other independent methods in other wavelength regions. Moreover, the FUV-derived accretion rates of individual systems can be compared with FUV-derived accretion rates of other systems in the same dwarf nova subclass or across subclasses. A number of implications and conclusions arise from this analysis.

Overall, the steady state, optically thick disk model fits to the outburst spectra shown in Figures 1 through 8 are quite acceptable and in some cases excellent. All of the accretion rates derived from the FUV fall within the range 1×10^{-8} to $1 \times 10^{-9} M_{\odot} \text{yr}^{-1}$ for the distances, white dwarf masses, orbital inclinations, and reddening values we have adopted. Therefore, the main uncertainties in the derived accretion rates, or in constraining the outburst accretion rates, arise from the uncertainties in the published values of the white dwarf masses, the orbital inclinations and the reliability of the distances.

On the other hand, there are several systems with outburst spectra in the IUE archive that merit attention because they differ significantly from the FUV energy distribution of steady state accretion disks. Aside from the eclipsing systems Z Cha and OY Car, which reside below the period gap and are seen nearly edge-on with absorbing curtains, all of the systems that depart from a steady state disk distribution do so longward of 1600Å and all of these systems lie above the period gap except for T Leo. The U Gem-type and Z Cam-type systems are WX Hyi, YZ Cnc, RX And, AH Her, Z Cam, EM Cyg, RU Peg, SY Cnc, DX And, and BV Cen.

If one takes our FUV-derived accretion rates in outburst at face value, then in principle

they can be used in combination with accretion rates derived for dwarf nova quiescence, and the timescales of outburst and quiescence to estimate the time-averaged accretion rate of the system during its lifetime as a dwarf nova. That is, when average accretion rates are known during quiescence and during outburst, then a true time-averaged accretion rate or mean accretion rate, $\langle \dot{M} \rangle$, may be derived. If \dot{M}_{ob} is an average accretion rate in outburst, \dot{M}_q is an average accretion rate in quiescence, t_{ob} is the average duration of outburst and t_q is the average duration of quiescence, then for a dwarf nova duty cycle

$$t_{tot} = t_{ob} + t_q \quad (4)$$

the "duty-cycle" averaged \dot{M} is given by

$$\langle \dot{M} \rangle = [\dot{M}_{ob}t_{ob} + \dot{M}_qt_q]t_{tot}^{-1} \quad (5)$$

Now it appears that all dwarf novae both above and below the gap have $\dot{M} = 10^{-8}$ to $10^{-9}M_{\odot}\text{yr}^{-1}$ in outburst. Suppose we assume the outburst times and quiescence times as well as the WD masses of all dwarf novae are the same. Then the only possible causes for a difference in accretion heating of a WD in a DN above the gap compared with a WD below the gap are: (1) a difference in WD ages due to evolution age; (2) a different amount of disk accretion during the outburst (i.e. more mass from the disk accreted above the gap versus the mass fraction of the disk accreted below the gap) or; (3) a significantly higher accretion rate during quiescence for DN above the gap than below the gap. Looking at the above equation, if \dot{M}_q is sufficiently high and the quiescence long enough (as in many long period dwarf novae), then the second term in equation (4) can compete and possibly overwhelm the first term if the outburst duration is short enough, if \dot{M}_{ob} is lower, say, less than $10^{-9}M_{\odot}\text{yr}^{-1}$, or if the accretion rate during quiescence is higher than a nominal $1 \times 10^{-11}M_{\odot}\text{yr}^{-1}$ that we assume in this paper.

While the above time-averaged accretion rate are gotten directly from model-derived accretion rates, the time-averaged accretion rates derived for selected dwarf novae by Patterson (1984) were obtained for the most part from a mean optical brightness level in AAVSO light curves on the assumption that the accretion disk is the sole source of the system light. By converting the mean magnitude to a flux and combining it with an estimated distance, a luminosity was obtained. The accretion rate providing that luminosity was derived for a given assumed or known white dwarf mass.

It is of interest to carry out a quantitative comparison of the two approaches to estimating $\langle \dot{M} \rangle$. For illustration, we take sample values for the outburst timescale and the recurrence timescale of a typical dwarf nova. We assume for simplicity that the recurrence time of dwarf nova outbursts is constant at, say 21 days, and the outburst timescale is constant at 7 days. For these parameters, if the outburst accretion rate is $10^{-8}M_{\odot}\text{yr}^{-1}$ then,

by (1), $\langle \dot{M} \rangle = 2.5 \times 10^{-9} \text{M}_{\odot} \text{yr}^{-1}$. If the outburst accretion rate is $10^{-9} \text{M}_{\odot} \text{yr}^{-1}$ and the quiescent rate is assumed to be $1 \times 10^{-11} \text{M}_{\odot} \text{yr}^{-1}$, then $\langle \dot{M} \rangle = 2.5 \times 10^{-10} \text{M}_{\odot} \text{yr}^{-1}$.

Suppose we take average values of t_{ob} and t_q for two well-studied systems such as U Gem and SS Cygni. For U Gem, from Table 2, we take \dot{M}_{ob} to be $2 \times 10^{-8} \text{M}_{\odot} \text{yr}^{-1}$, t_{ob} of 14 days (wide outburst), t_q of 100 days and \dot{M}_q of $1 \times 10^{-11} \text{M}_{\odot} \text{yr}^{-1}$. Hence for these parameters U Gem would have $\langle \dot{M} \rangle \simeq 2.5 \times 10^{-9} \text{M}_{\odot} \text{yr}^{-1}$. Considering SS Cygni with the same quiescence accretion rate, t_{ob} of 14 days, t_q of 40 days and \dot{M}_{ob} of $3 \times 10^{-9} \text{M}_{\odot} \text{yr}^{-1}$ from Table 2, we find that $\langle \dot{M} \rangle \sim 7 \times 10^{-10} \text{M}_{\odot} \text{yr}^{-1}$.

Patterson (1984) estimated $\langle \dot{M} \rangle \simeq 3 \times 10^{-10} \text{M}_{\odot} \text{yr}^{-1}$ for U Gem and $\langle \dot{M} \rangle \sim 5 \times 10^{-10} \text{M}_{\odot} \text{yr}^{-1}$ for SS Cygni. We note that the distances adopted by Patterson (1984), 78 pc and 95 pc for U Gem and SS Cygni respectively, are closer than the FGS parallax distances we used for the two systems. Comparing Patterson’s values with the time-averaged accretion rates estimated using Table 2, our value of $\langle \dot{M} \rangle$ for U Gem is 10 times higher than estimated in Patterson (1984) while for SS Cygni, our $\langle \dot{M} \rangle$ is 1.4 times higher than the value estimated by Patterson (1984). Until the accretion rates during dwarf nova quiescence are more accurately known, it is premature to compute the time-averaged accretion rates in this direct manner. Moreover, individual accretion rates will not be secure for dwarf novae until there is further progress in determining better white dwarf masses, orbital inclinations and distances.

We are grateful to an anonymous referee for helpful comments. This work was supported by NSF grant AST05-07514, NASA grant NNG04GE78G and by summer undergraduate research support from the Delaware Space Grant Consortium. Some or all of the data presented in this paper were obtained from the Multimission Archive at the Space Telescope Science Institute (MAST). STScI is operated by the Association of Universities for Research in Astronomy, Inc., under NASA contract NAS5-26555. Support for MAST for non-HST data is provided by the NASA Office of Space Science via grant NAG5-7584 and by other grants and contracts.

REFERENCES

- Bruch, A., & Engel, A. 1994, A&A Suppl.Ser., 104, 79
- Harrison, T. et al. 2004, AJ, 127, 460
- Hamilton, R., & Sion, E.M., 2004, PASP, 116, 926
- Horne, K., & Cooke, M.C., 1985, MNRAS, 214, 307
- Hubeny, I. 1988, Comput. Phys. Comun., 52, 103
- Hubeny, I., & Lanz, T. 1995, ApJ, 439, 875
- Kiplinger, A.1979, ApJ, 234, 997
- la Dous, C. 1991, A&A, 252, 100
- Massa, F., & Fitzpatrick, E. 2000, ApJS, 126, 517
- Morales-Rueda, L. & Marsh, T., 2002, MNRAS, 332, 814
- Osaki, Y.2005, Proc.Japan Acad.,Ser.B, 81, 291
- Patterson, J.1984, ApJS, 54, 443
- Polidan, R., Mauche, C., & Wade, R.1990, ApJ, 356, 211
- Polidan, R., & Holberg, J., 1984, Nature, 309, 528
- Pringle, J. 1981, ARAA, 19, 137
- Pringle, J., & Verbunt, F. 1984, ESA SP-281
- Ritter, H., & Kolb, U. 1998, A&A, 129, 83
- Rutten, R.G.M., et al.1992, A&A, 260, 213
- Sion, E.M., et al.2003, ApJ, 592, 1137
- Smak, J. 1984, Acta Astr. 34, 161
- Smak, J. 1984, PASP, 96, 5
- Smak, J. 1989, Acta Astr., 39, 201
- Smak, J. 1994, Acta Astr. 44, 59

Thorstensen, J., 2003, AJ, 126, 3017

Verbunt, F. 1987, A&A, 71, 339

Wade, R.A. & Hubeny, I. 1998, ApJ, 509, 350.

Warner, B. 1995, Cataclysmic Variable Stars (Cambridge: Cambridge Univ. Press)

Winter, L., & Sion, E.M. 2003, ApJ, 582, 352

Table 1. OBSERVING LOG

System	Data ID	Observation Date (yyyy-mm-dd)	Observation Time (UT)	Exposure Time (s)	Outburst-Quiescence Cycle
(1)	(2)	(3)	(4)	(5)	(6)
WZ Sge	SWP03507	1978-12-01	19:21:00	24	Peak Outburst
SW UMa	SWP27871	1986-03-08	04:32:00	210	Outburst
WX Cet	SWP36511	1989-06-15	10:41:00	3300	Late Decline
T Leo	SWP33642	1988-05-25	20:53:00	300	Outburst
V1159 Ori	SWP56889	1996-03-03	17:01:00	5400	Rise to Outburst
V436 Cen	SWP54246	1995-03-28	10:09:00	2400	Outburst *
BC UMa	SWP50668	1994-05-01	21:09:00	3000	Peak Outburst
EK TrA	SWP09705	1980-08-05	22:20:00	1140	Outburst *
TV Crv	SWP41842	1991-06-14	14:25:00	1800	Outburst *
OY Car	SWP25838	1985-05-02	17:34:00	720	Rise to Outburst
VY Aqr	SWP21720	1983-12-08	03:22:00	600	Outburst
ER UMa	SWP40947	1991-02-27	22:20:00	4500	Outburst *
IR Gem	SWP38524	1990-04-05	02:03:00	1068	Outburst
AY Lyr	SWP09342	1980-06-22	06:46:00	3600	Late Outburst
VZ Pyx	SWP44129	1992-03-07	05:36:00	2400	Outburst *
VW Hyi	SWP40045	1990-11-04	10:45:00	150	Peak Outburst
Z Cha	SWP30670	1987-03-31	17:03:00	600	Peak Outburst
WX Hyi	SWP23952	1984-09-13	19:22:00	3600	Outburst *
SU UMa	SWP35261	1989-01-05	08:58:00	1800	Peak Outburst
YZ Cnc	SWP15560	1981-11-24	10:07:00	540	Outburst
TU Men	SWP10665	1980-11-23	17:58:00	1800	Outburst *
AB Dra	SWP07413	1979-12-15	18:51:00	4500	Rise to Outburst
CY Lyr	SWP21030	1983-09-12	22:09:00	3600	Outburst
KT Per	SWP07382	1979-12-13	01:19:00	2700	Early Decline
AR And	SWP15445	1981-11-07	12:34:00	2100	Outburst
CN Ori	SWP15950	1982-01-04	08:36:00	2400	Outburst
X Leo	SWP15985	1982-01-06	14:03:00	6240	Outburst
VW Vul	SWP18875	1982-12-23	19:08:00	7200	Transition *
UZ Ser	SWP15078	1981-09-22	18:41:00	2400	Outburst
U Gem	SWP10327	1980-10-10	13:28:00	353	Peak Outburst
TW Vir	SWP10951	1981-01-03	06:47:00	3600	Outburst *
SS Aur	SWP18610	1982-11-20	17:33:00	1560	Rise to Outburst
HX Peg	SWP37459	1989-10-25	19:31:00	3600	Outburst *
RX And	SWP17678	1982-08-13	22:59:00	600	Peak Outburst
CZ Ori	SWP16039	1982-01-14	03:18:00	2700	Outburst
AH Her	SWP17662	1982-08-11	22:12:00	1200	Outburst
TZ Per	SWP17643	1982-08-09	19:37:00	2580	Outburst
TT Crt	SWP47805	1993-06-04	19:54:00	3300	Outburst
SS Cyg	SWP47746	1993-05-27	07:57:00	180	Outburst
Z Cam	SWP21721	1983-12-08	05:41:00	240	Early Decline
EM Cyg	SWP07297	1979-12-02	22:45:00	1500	Outburst
RU Peg	SWP15079	1981-09-22	20:43:00	840	Decline
SY Cnc	SWP07313	1979-12-05	00:40:00	1200	Mid Decline
DX And	SWP37687	1989-11-26	15:25:00	2700	Rise to Outburst
WW Cet	SWP10664	1980-11-23	16:21:00	1800	Transition *
BV Cen	SWP24867	1985-01-08	20:48:00	3600	Transition *

Table 1. Sample stars and associated SWP spectra listed by increasing orbital period. An asterix in the final column denotes that the cycle state was determined in the absence of an optical light curve as described in §2.

Table 2. SYSTEM PARAMETERS

Reference Number (1)	System (2)	Sub Type (3)	Orbital period (days) (4)	Reddening (5)	Distance (pc) (6)	i ($^{\circ}$) (7)	\dot{M} ($M_{\odot}\text{yr}^{-1}$) (8)	WD % (9)	Disk % (10)
01	WZ Sge	SU-WZ	0.056687846	0.00	43.3 π	78	2.5×10^{-8}	≤ 0.5	≥ 99.5
02	SW Uma	SU(DQ?)	0.056815	0.00	110	60	3.2×10^{-9}	0	100
03	WX Cet	SU-WZ	0.05827	0.00 ?	187	41	1.0×10^{-9}	0	100
04	T Leo	SU	0.05882	0.00	101 π	60	1.0×10^{-8}	0	100
05	V1159 Ori	SU-ER	0.06217801	0.00 ?	213	60	1.0×10^{-9} :	0	100
06	V436 Cen	SU	0.062501	0.05; 0.00	320	41	2.2×10^{-9}	1	99
07	BC Uma	SU-WZ	0.06261	0.00 ?	285	75	3.2×10^{-9}	0	100
08	EK TrA	SU	0.06288	0.05; 0.00	200	18	9.0×10^{-10} :	≤ 1	≥ 99
09	TV Crv	SU	0.0629	0.00	268	60	1.0×10^{-9}	0	100
10	OY Car	SU	0.062917	0.00	85	75	6.0×10^{-9}	≤ 11	≥ 89
11	VY Aqr	SU-WZ	0.06309	0.00	97 π	41	1.0×10^{-9}	0	100
12	ER Uma	SU-ER	0.06366	0.00 ?	460	60	9.0×10^{-9} :	≤ 1	≥ 99
13	IR Gem	SU	0.0684	0.00	250	60	1.0×10^{-8}	0	100
14	AY Lyr	SU	0.0737	0.00	380	41	3.2×10^{-9}	0	100
15	VZ Pyx	SU (IP?)	0.07332	0.00	280	60	2.8×10^{-9}	5	95
16	VW Hyi	SU	0.074271	0.00	65	60	3.2×10^{-9}	0	100
17	Z Cha	SU	0.074499	0.00	97	81	4.0×10^{-9} :	≤ 19	≥ 81
18	WX Hyi	SU	0.0748125	0.00	280	60	1.0×10^{-9}	1	99
19	SU Uma	SU	0.07635	0.00	270 π	41	7.0×10^{-10}	2	98
20	YZ Cnc	SU	0.0868	0.00	265 π	41	2.5×10^{-9}	≤ 2	≥ 98
21	TU Men	SU	0.1172	0.08	320	41	1.0×10^{-8}	0	100
22	AB Dra	ZC	0.15198	0.10	400	81	1.0×10^{-9}	8	92
23	CY Lyr	UG	0.1591	0.18	400	60	1.0×10^{-8}	0	100
24	KT Per	ZC	0.16265777	0.15-0.54; 0.2	245	60	2.2×10^{-9}	≤ 0.5	≥ 99.5
25	AR And	UG (SU?)	0.16302	0.02	270	60	1.0×10^{-8} :	0	100
26	CN Ori	UG	0.163199	0.00	295	60	9.0×10^{-9}	2	98
27	X Leo	UG	0.1646	0.00	350	41	3.2×10^{-10}	12	88
28	VW Vul	ZC	0.16870	0.15	650	41	1.0×10^{-8}	19	81
29	UZ Ser	UG (ZC?)	0.173	0.35	300	18	2.0×10^{-8}	1	99
30	WW Cet	UG (ZC?)	0.1758	0.00	190	60	1.0×10^{-9} :	≤ 1	≥ 99
31	U Gem	UG	0.17690619	0.00-0.05; 0	96 π	75	1.6×10^{-8}	1	99
32	TW Vir	UG	0.18267	0.00	500	60	2.8×10^{-9} :	≤ 1	≥ 99
33	SS Aur	UG	0.1828	0.10	201 π	41	7.0×10^{-9} :	≤ 0.5	≥ 99.5
34	HX Peg	...	0.2008	0.00	550(π)	41	2.8×10^{-9} :	≤ 8.5	≥ 91.5
35	RX And	ZC	0.209893	0-0.06; 0	200	41	2.0×10^{-9}	1.5	98.5
36	CZ Ori	UG	0.214667	0.00	260	18	3.0×10^{-10} :	≤ 14	≥ 86
37	AH Her	ZC	0.258116	0.3	660 π	41	9.0×10^{-9} :	≤ 0.5	≥ 99.5
38	TZ Per	ZC	0.262906	0.27	275	41	6.0×10^{-9}	5	95
39	TT Crt	UG	0.2683522	0.00	500	60	3.0×10^{-9} :	≤ 3	≥ 97
40	SS Cyg	UG	0.27513	0.04; 0	166 π	18	3.2×10^{-9}	≤ 0.5	≥ 99.5
41	Z Cam	ZC	0.2898406	0.0-0.06; 0	112 π	60	9.0×10^{-10}	1	99
42	EM Cyg	ZC	0.290909	0.05; 0	350	75	7.0×10^{-9}	≤ 0.5	≥ 99.5
43	RU Peg	UG	0.3746	0.00	282 π	41	1.0×10^{-9}	0	100
44	SY Cnc	ZC	0.38	0.00	450	18	1.0×10^{-8}	0	100
45	DX And	UG	0.440502	0.00	500	60	1.0×10^{-8}	7	93
46	BV Cen	UG	0.610108	0.05-0.36; 0.1	500	60	3.2×10^{-9}	≤ 0.5	≥ 99.5

Table 2. Sample stars listed by increasing orbital period. A reference number is given to each system to locate the associated fit in the accompanying figures.

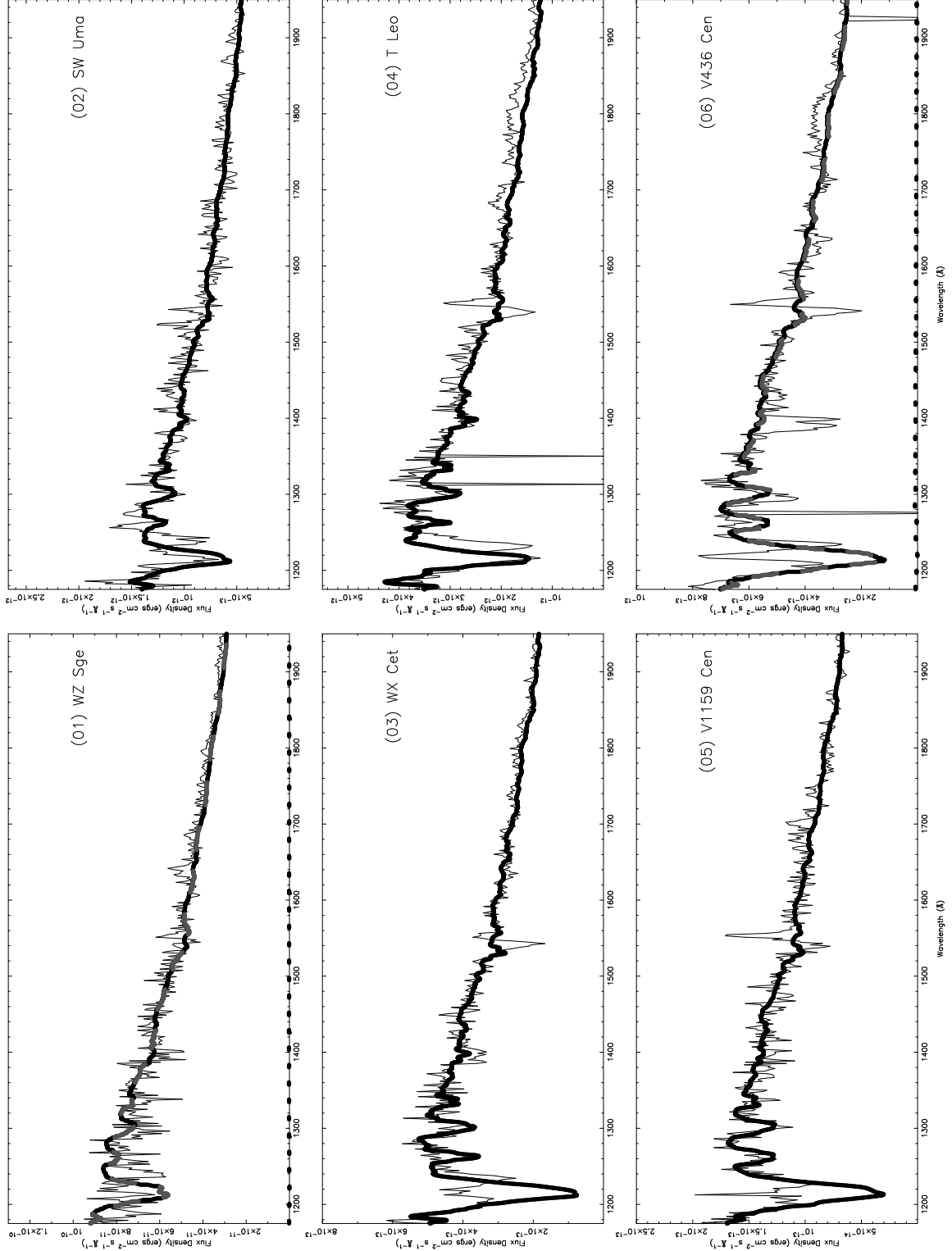


Fig. 1.— Flux density versus wavelength plots for (01) WZ Sge, (02) SW UMa, (03) WX Cet, (04) T Leo, (05) V1159 Cen, (06) V436 Cen. The best fitting accretion disk model is shown with the thick solid line. If in rare cases a hot WD model was added to the best-fit accretion disk to try to improve the fit, then the WD model flux is denoted by a dotted line, the accretion disk model flux alone by a dashed line and the combined flux by a thick solid line. All very sharp narrow absorption features seen extending down to zero flux level

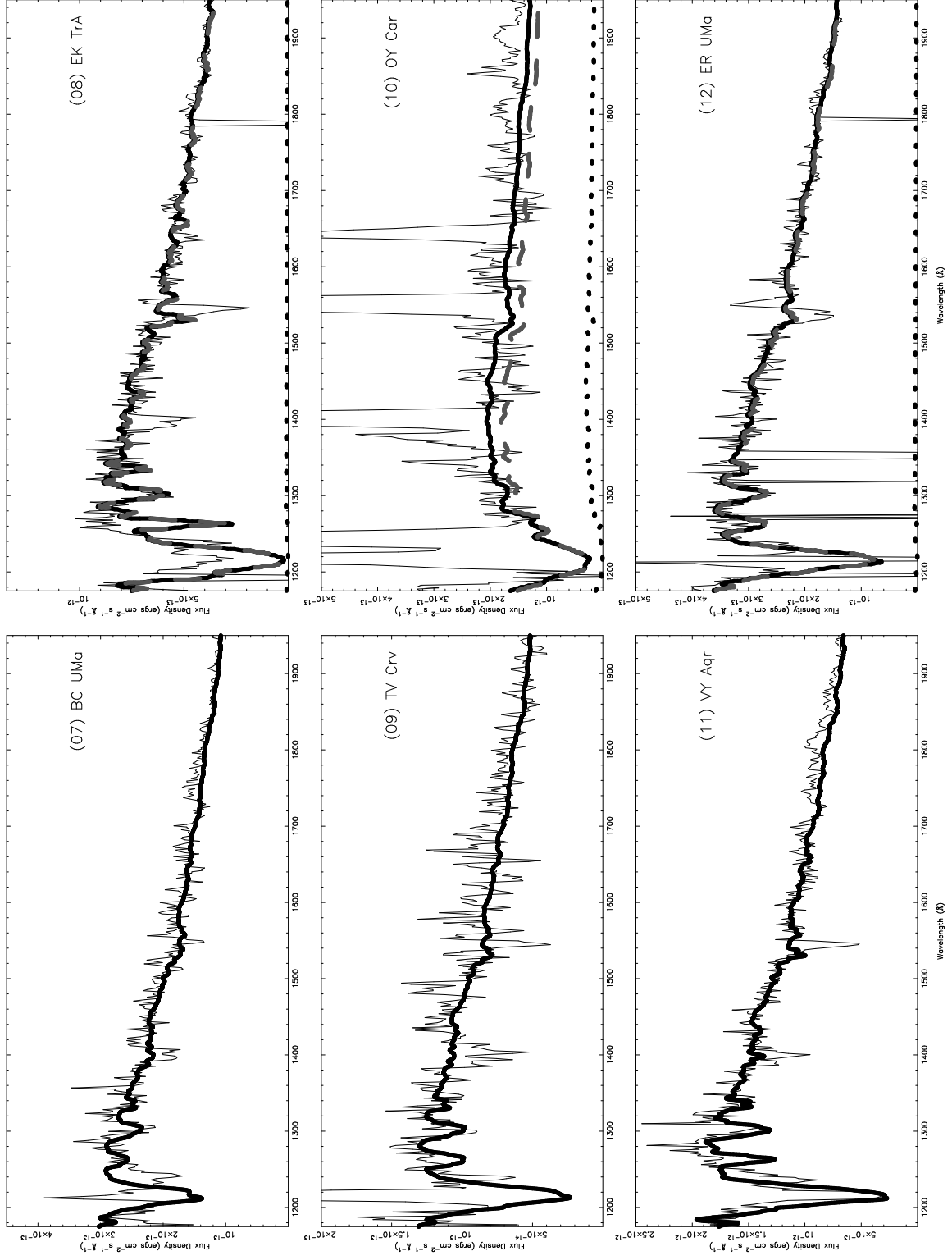


Fig. 2.— Same as Figure 1 except for (07) BC UMa, (08) EK Tra, (09) TV Crv, (10) OY Car, (11) VY Aqr, (12) ER UMa

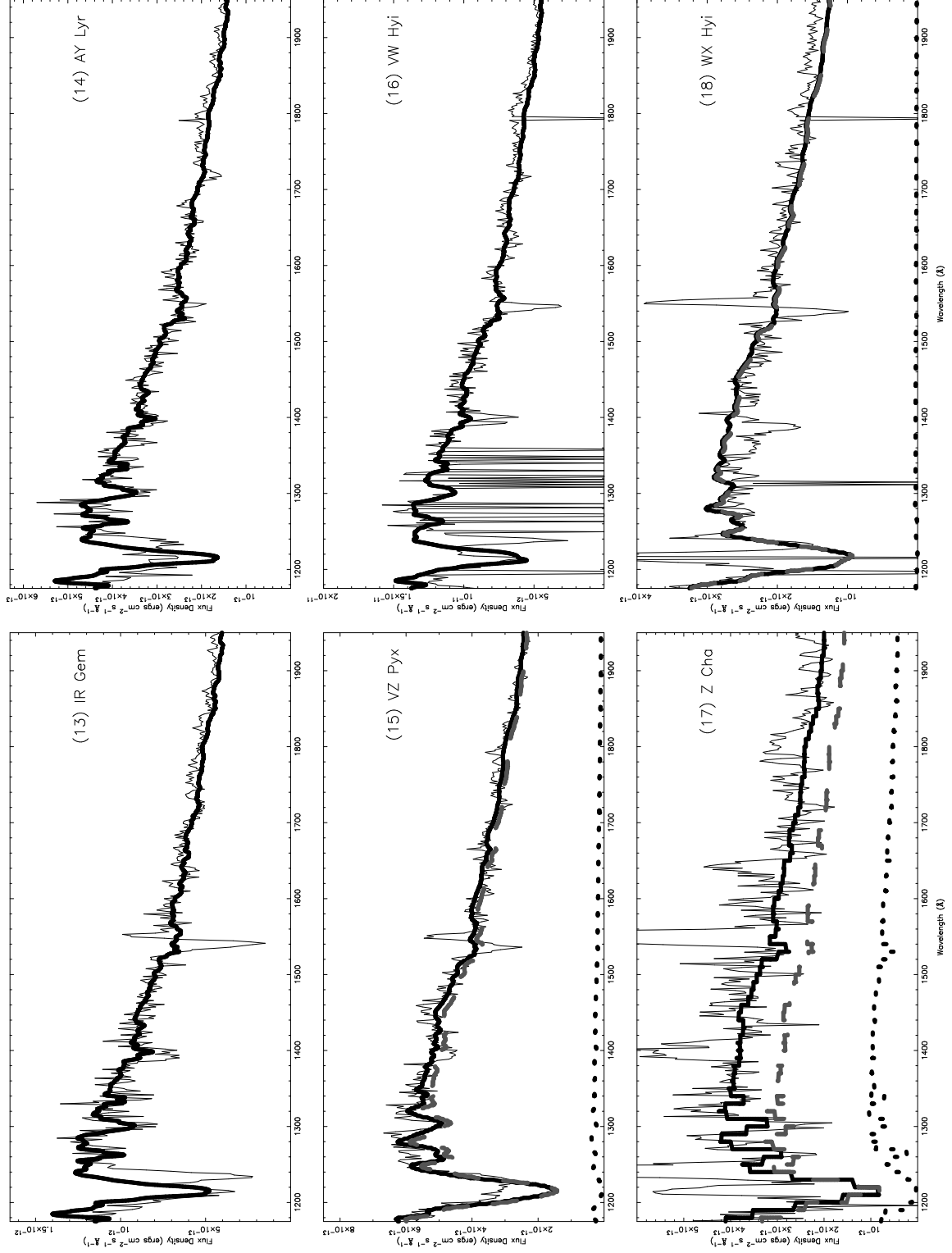


Fig. 3.— Same as Figure 1 except for (13) IR Gem, (14) AY Lyr, (15) VZ Pyx, (16) VW Hyi, (17) Z Cha, (18) WX Hyi

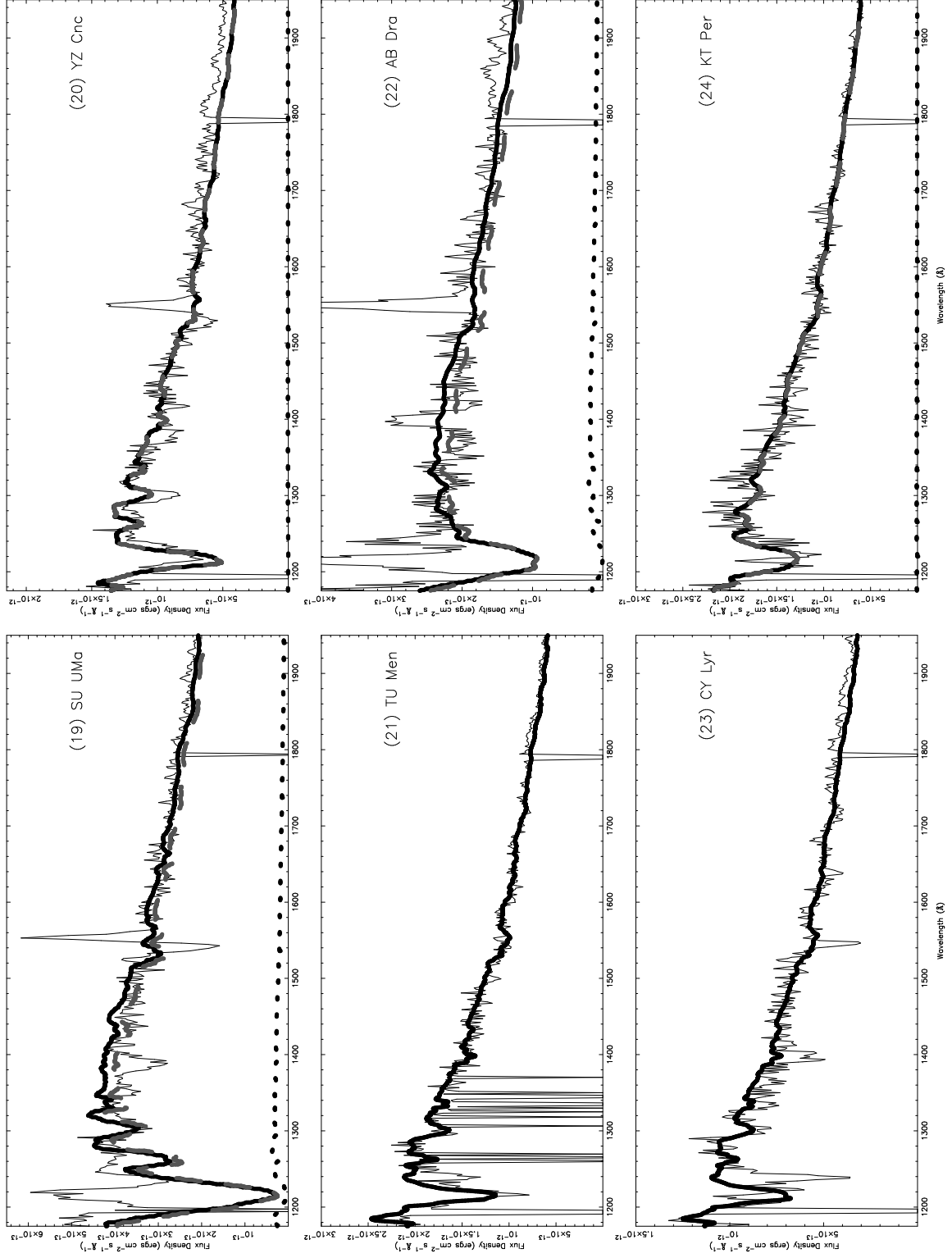


Fig. 4.— Same as Figure 1 except for (19) SU UMa, (20) YZ Cnc, (21) TU Men, (22) AB Dra, (23) CY Lyr, (24) KT Per

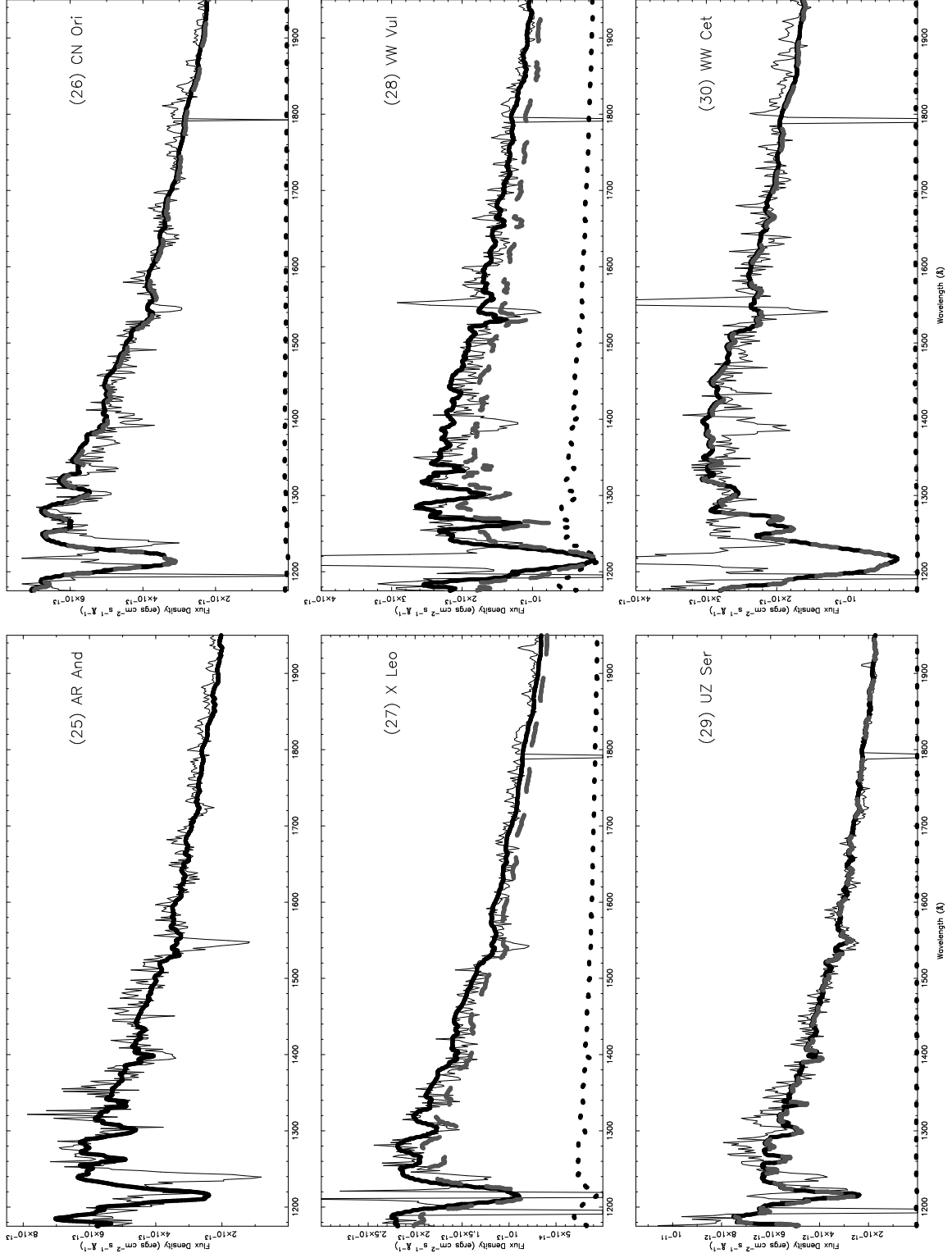


Fig. 5.— Same as Figure 1 except for (25) AR And, (26) CN Ori, (27) X Leo, (28) VW Vul, (29) UZ Ser, (30) WW Cet

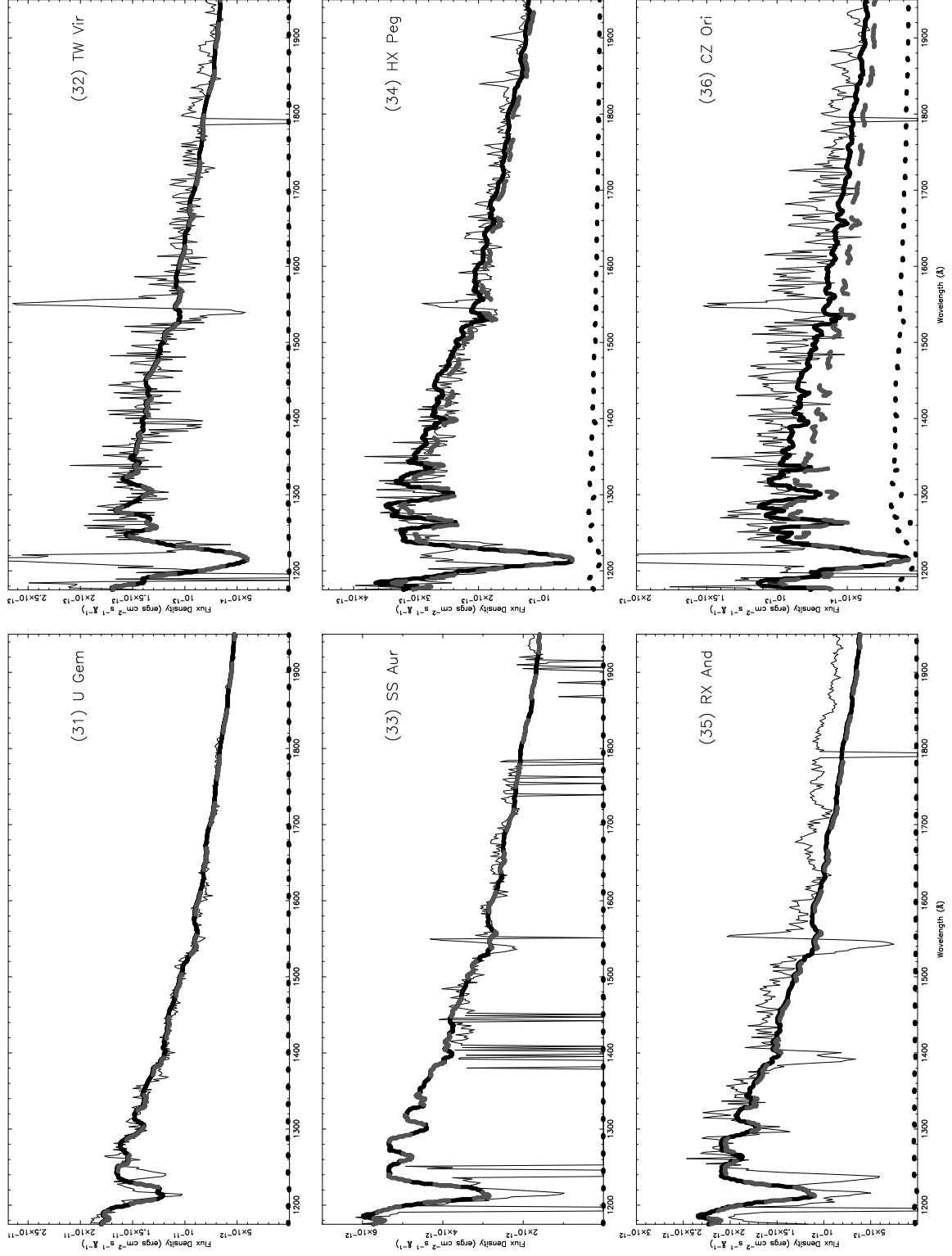


Fig. 6.— Same as Figure 1 except for (31) U Gem, (32) TW Vir, (33) SS Aur, (34) HX Peg, (35) RX And, (36) CZ Ori

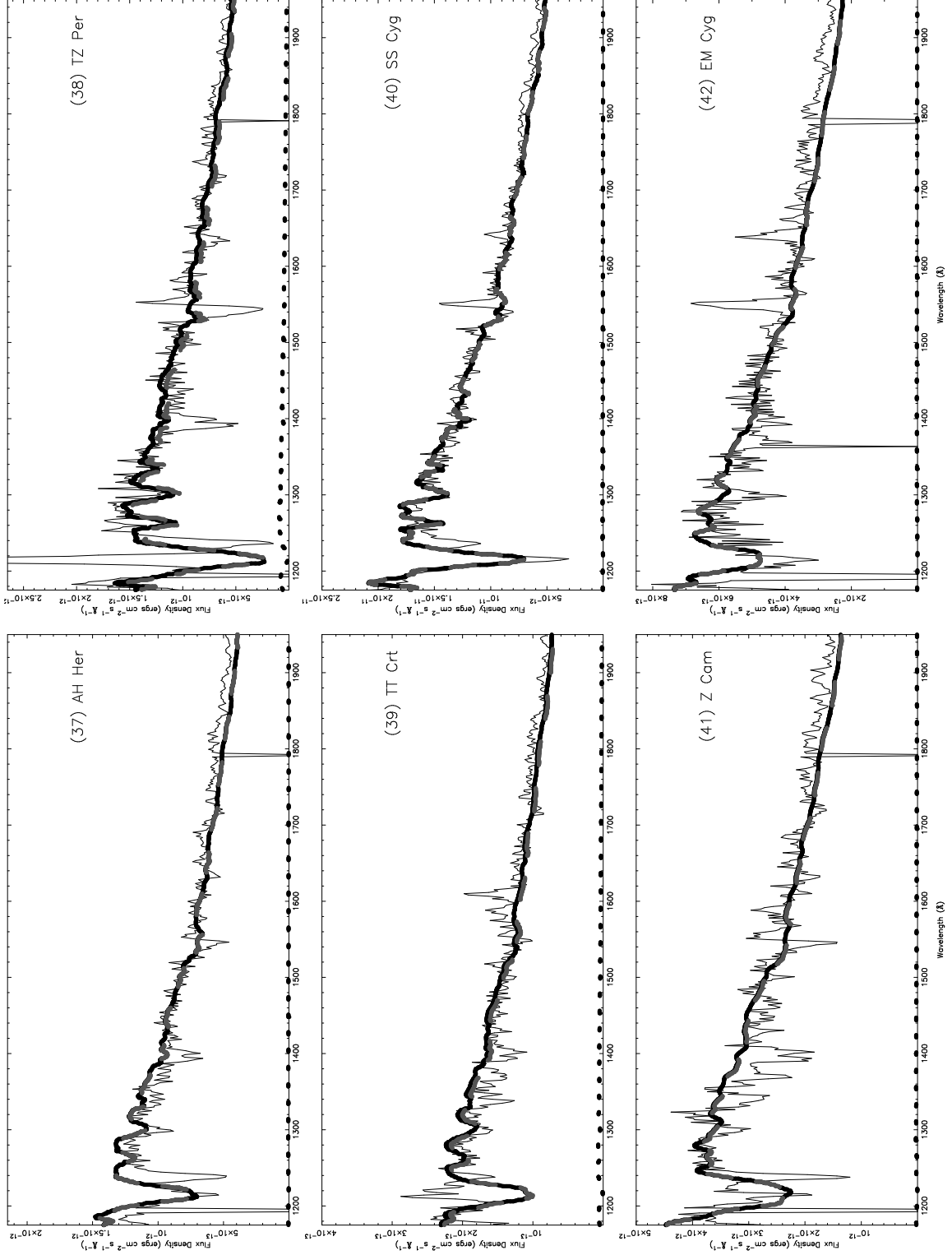


Fig. 7.— Same as Figure 1 except for (37) AH Her, (38) TZ Per, (39) TT Crt, (40) SS Cyg, (41) Z Cam, (42) EM Cyg

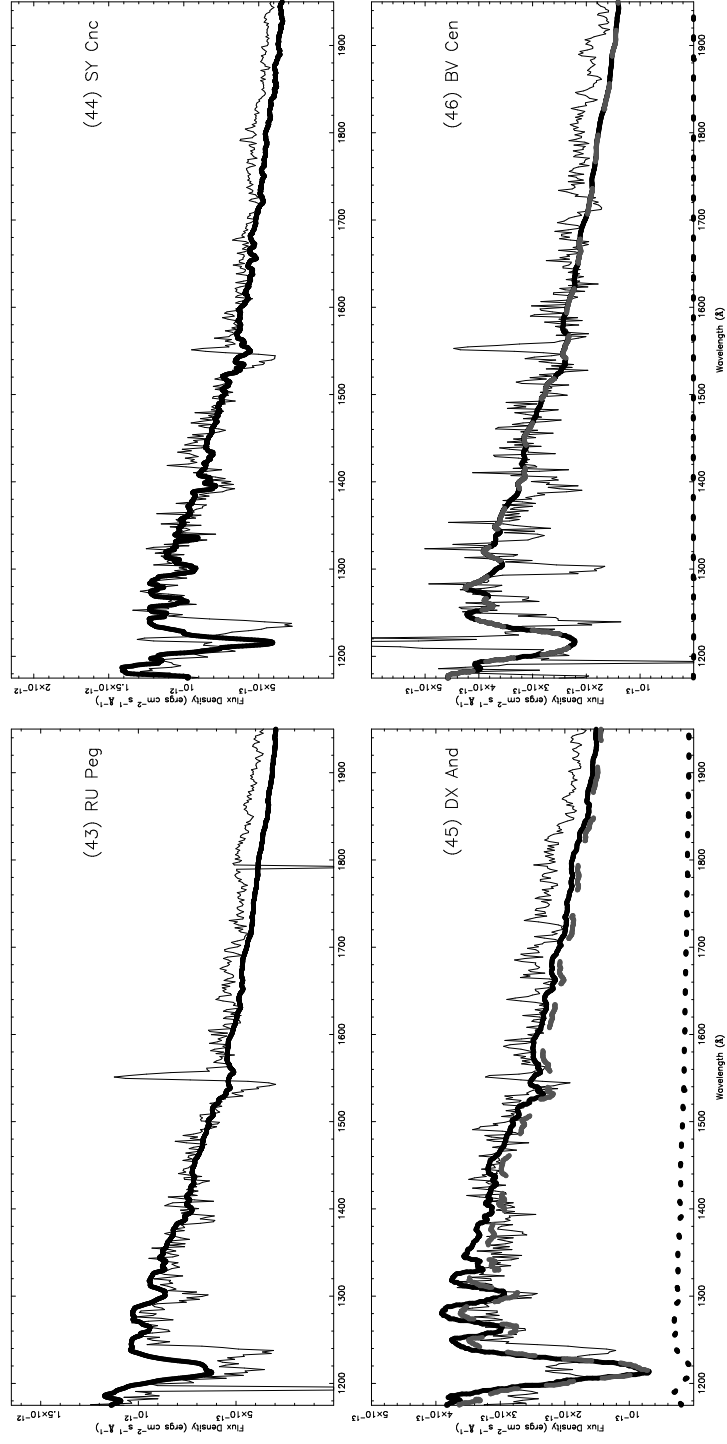


Fig. 8.— Same as Figure 1 except for (43) RU Peg, (44) SY Cnc, (45) DX And, (46) BV Cen